Earthquake Geotechnical Engineering for Protection and Development of Environment and Constructions – Silvestri & Moraci (Eds)
© 2019 Associazione Geotecnica Italiana, Rome, Italy, ISBN 978-0-367-14328-2

Effects of dynamic soil-structure interaction on the performance of structures equipped with viscous dampers

J.I. Boksmati & S.P.G. Madabhushi
Schofield Centre, Department of Engineering, University of Cambridge, Cambridge, UK

N.I. Thusyanthan
Atkins, UK

ABSTRACT: Viscous dampers are common energy dissipation devices installed in superstructures to minimise seismic induced story shears and drifts. Most of the experimental research into the performance of buildings with viscous dampers fail to capture the realistic behaviour of soil-structure interaction (SSI) in the field. This paper presents one of the first experimental attempts to investigate the effects of SSI on the performance of damped sway frames through dynamic centrifuge testing. The paper will show the successful application of model oil dampers in the centrifuge and compare the response of a model damped frame to a similar frame without dampers. The degree of SSI was varied by varying the intensity of the input motions. Hysteretic damping of soil beneath the foundations is found to increase the effective damping in both damped and undamped frames. The ground compliance triggers global rocking in the damped frame which can limit damper performance.

1 INTRODUCTION

Design engineers often resort to two classical strategies for achieving seismic performance objectives during building design. The first approach limits seismic induced story drifts through the provision of adequate stiffness in the superstructure. This method ensures satisfactory floor displacements at the expense of higher floor accelerations and member forces in the frame. The other procedure to reducing seismic demand is by allowing for controlled plasticity to occur at specific locations in the superstructure. This rigours method maximises the efficiency of the chosen structural sections in the frame at the cost of higher story drifts and permanent damage. Ongoing research into earthquake engineering has expanded the tools currently available to seismic engineers. One innovative solution to this end is the incorporation of supplemental energy dissipation devices into the superstructure. Velocity-dependant devices, specifically viscous dampers or oil dampers, are unique in this field as they allow for simultaneous reductions in floor accelerations, story forces, and story drifts, without significant alteration to the stiffness of the superstructure.

Ever since the introduction of viscous dampers into the commercial markets in the early 1990s (Lee & Taylor 2001), numerous large-scale shaking-table programs have been commissioned to better understand the seismic behaviour of buildings equipped with viscous dampers (Seleemah & Constantinou 1997, Chang et al. 2008, Ji et al. 2013). Unfortunately, the majority of these tests utilised multi-story test-frames in which the ground columns were anchored into stiff shaking tables to achieve rigid base fixity. It is well established that ground compliance beneath a structure can introduce a global rocking mode which would occur simultaneously with floor sway in the event of an earthquake. This global response, accompanied with energy dissipation brought about by the hysteretic foundation soil material, can indeed change the behaviour and efficiency of a damped building in the event of a real earthquake. A review of current literature reveals very limited efforts towards evaluating the effects of soil-structure

interaction (SSI) on the performance of buildings with viscous dampers. Analytical and numerical studies into this field have hinted towards a drop in damper efficiency as SSI becomes more significant (Chuanromanee et al. 1995, Zhou et al. 2012, Li et al. 2015). Nevertheless, these studies are not without their rudimentary simplifications of material and geometrical nonlinearities that would occur at the foundation soil interface. The work presented in this paper marks the first experimental effort in this field to investigate the effects of SSI on the performance of buildings equipped with viscous dampers.

2 PHYSICAL MODELLING

Dynamic centrifuge testing presents itself as a very powerful tool for investigating dynamic soil-structure interaction problems. The ability of a centrifuge model to capture the realistic dynamic soil impedance beneath a building's foundation allows researchers to replicate real soil constitutive behaviours and possible geometrical nonlinearities (i.e. footing uplift) without the need for analytical simplifications. This model-to-prototype scaling is mainly possible due to the one-to-one scaling of soil stresses and strains at specific points between the centrifuge soil model and the prototype soil domain. The centrifuge package was prepared at a scale of 1:50, then tested at 50g for different base excitations using the servo-hydraulic earthquake actuator developed by Madabhushi et al. (2012). All results presented herein, unless otherwise stated, are at prototype scale, following the well-established centrifuge scaling laws summarised in Madabhushi (2014).

2.1 *Model structures*

Two very similar two-degree-of-freedom model sway frames have been fabricated from 6082-T6 aluminium alloy plates to the dimensions shown in Figure 1. One frame was equipped with horizontal miniature oil dampers, while the other frame was kept bare for comparison. Given the relative small story drifts in the centrifuge (in the order of few millimetres model scale), the oil dampers have been positioned horizontally on each floor to maximise input into the dampers. A squatty aspect ratio was selected for the frames to maximise floor sway (i.e. damper input) and reduce possible rocking during shaking. Table 1 gives details of the two model frames under investigation.

Miniature oil dampers in the centrifuge are subjected to drastically different operating conditions than their counterparts in prototype structures. The scaling-up of frequency in dynamic centrifuge tests implies that the miniature dampers will have to respond to very high frequencies and under very small strokes. Further discussion on the challenges of developing model dampers can be found in Boksmati et al. (2018).

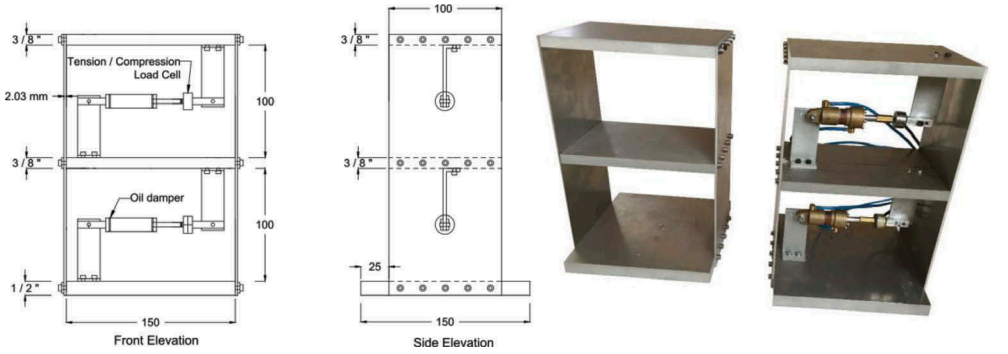

Figure 1. Details of the centrifuge model frames. All dimensions are in mm unless otherwise noted.

Table 1. Model frame properties.

	Bare Frame		Damped Frame	
	Model scale	Prototype scale	Model scale	Prototype scale
Mode 1	41.7 Hz	0.83 Hz	42 Hz	0.84 Hz
Mode 2	114.0 Hz	2.28 Hz	-	-
Damping fluid	-		68 cst oil	
Bearing pressure	40 kPa		51 kPa	
Total mass	1.83 kg	228.75 tonnes	2.36 kg	294.89 tonnes
1st floor lumped mass	0.54 kg	67.575 tonnes	0.73 kg	91.675 tonnes
2nd floor lumped mass	0.47 kg	58.575 tonnes	0.66 kg	82.674 tonnes

2.2 *Centrifuge testing*

The damped and undamped sway frames are founded on raft foundations and embedded in dry loose Hostun sand (HN-31) which has been air-pluviated at a target relative density of 39 % using the automatic sand pourer described in Madabhushi et al. (2006). The frames were founded on such a loose sand deposit to increase the stiffness contrast between the buildings and the soil, thus triggering greater soil-structure interaction. Details of the sand properties can be found in Haigh et al. (2012). The sand was poured into an Equivalent Shear Beam (ESB) container which is described by Brennan et al. (2006). Figure 2 illustrates the overall layout of the centrifuge package and the instrumentation used. Arrays of piezo-electric accelerometers are buried in the sand to monitor vertically propagating shear waves during base excitations.

Both model frames are instrumented with micro-electro-mechanical-systems (MEMS) accelerometers to record foundation inputs, floor accelerations, and vertical accelerations. In the damped structure, each model damper was instrumented with two MEMS accelerometers, one on the damper body (D2 and D4) and one on the damper piston (D1 and D3) in addition to a tension/compression load cell to record damping forces. All acceleration and force data presented in this paper are filtered using a lowpass fourth order Butterworth filter at a frequency cut-off of 500 Hz (10 Hz prototype). Damper stroke information was obtained by taking the difference between the two MEMS accelerometers on each damper. Through double integration and high-pass filtering, damper stroke displacements were obtained from the acceleration data. All displacements and rotational data computed from MEMS accelerations have been band-pass filtered twice using a fourth order Butterworth filter with frequency cut-off points at 15 Hz and 500 Hz.

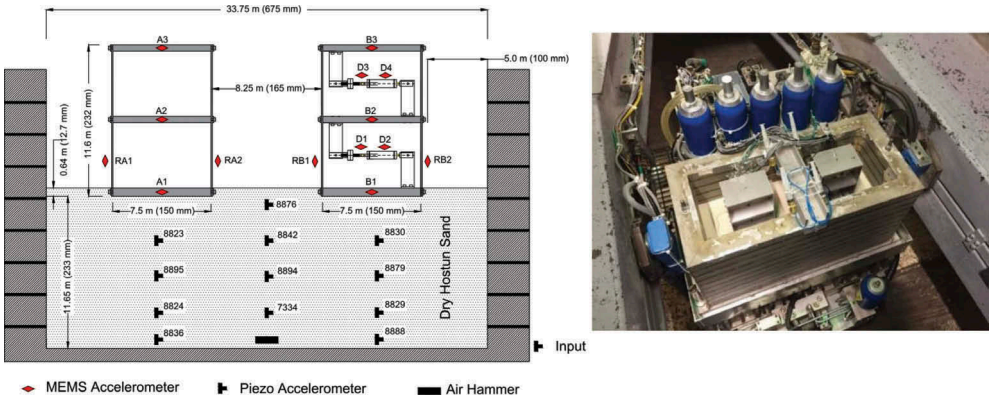

Figure 2. Instrumentation layout of the centrifuge model in prototype scale and model scale.

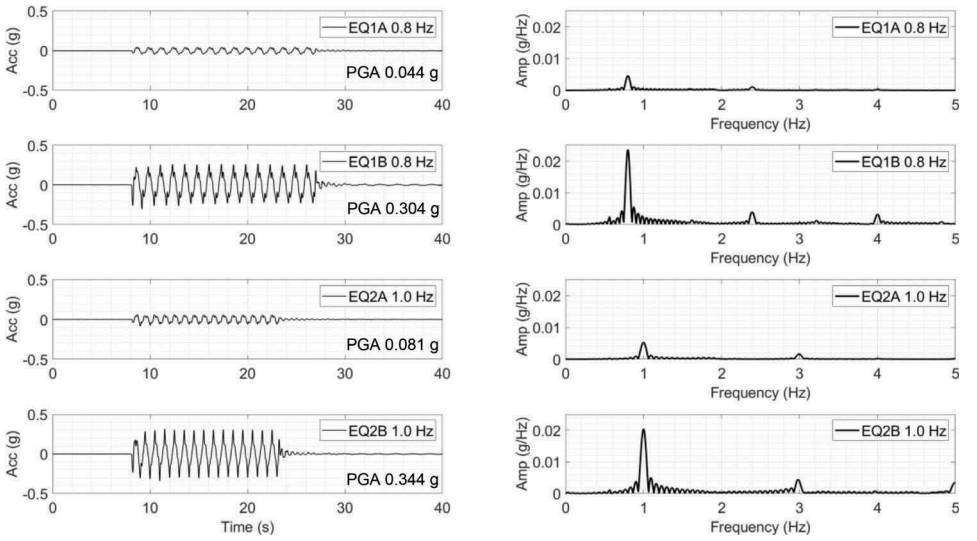

Figure 3. Prototype input accelerations.

2.3 *Input motions*

Four 15 cycle single-tone base motions have been selected for this investigation. The first sinusoidal input has a frequency of 0.8 Hz which is near the resonant frequency of the frames. Another 1 Hz input motion was triggered to investigate the response of the buildings to a base motion 1.25 times higher than resonance. The intensity of each these two sinusoidal motions was varied to trigger different degrees of SSI. It is important to mention that input motions EQ1A, EQ2A, EQ1B and EQ2B were triggered in succession during the same centrifuge test. Figure 3 shows the input motions recorded at the base of the ESB box.

3 DYNAMIC RESPONSE OF STRUCTURES

3.1 *Effects of miniature dampers on frame response*

Absolute floor accelerations for both frames are presented in Figure 4 for EQ1A and EQ2A respectively. The bare frame floor accelerations at 0.8 Hz show minor signs of beating. This is often typical of a flexible structure responding very close to its natural frequency. At the end of the base excitation, the bare frame seems to enter a long phase of free-vibration dominated by logarithmic decay. The miniature dampers in the damped frame are successful at mitigating peak roof accelerations from 0.68 g to 0.42 g for EQ1A, and have substantially shortened the free-vibration phase down to around 6 cycles. Traces of the second mode of the structure appear in the peak floor acceleration traces of the bare frame. This higher frequency is more dominant in the first floor free-vibration response. Interestingly, the acceleration traces for the damped frame show very little evidence of the second mode of the structure. For EQ2A, the reductions in peak absolute floor accelerations between the bare and the damped frame are not as significant. The free-vibration phase of the floor acceleration traces can be used to approximate the damping ratio of the frames using the concept of logarithmic decrement. From the roof acceleration traces, the damping ratio (ζ) of the damped frame is approximately 5.3 % compared to 0.6 % for the bare frame.

The instrumentation installed on the miniature dampers allow damper force-displacement loops to be generated for each earthquake. Figure 5 shows the model damper performance plots for the different base excitations tested. Ideally, linear viscous damper loops are elliptical in shape with maximum damping forces occurring at mid-stroke, and zero forces at the ends

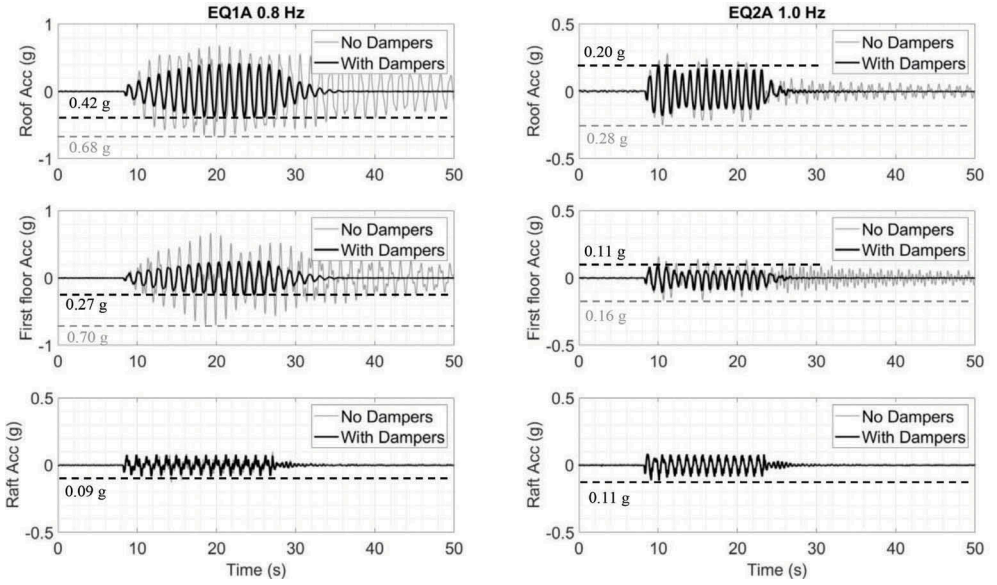

Figure 4. Absolute floor accelerations for the bare frame and damped frame for EQ1A and EQ2A.

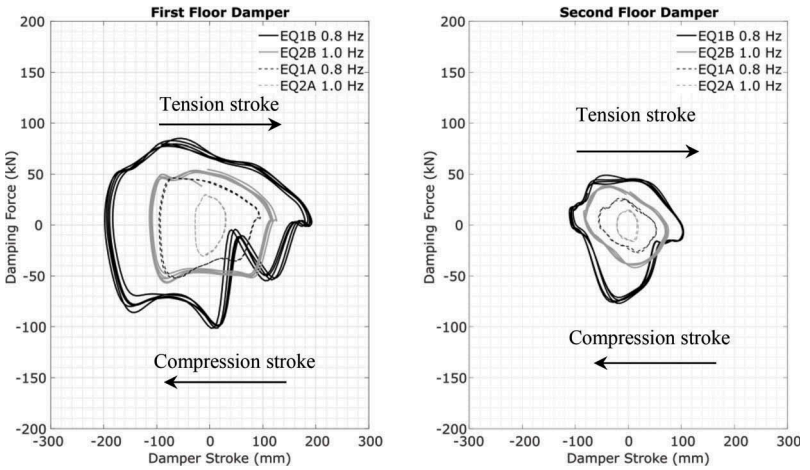

Figure 5. Damper force-displacement loops for the last 5 cycles of input motion.

of the damper stroke. The loops generated during EQ2A motion closely resemble that of an ideal viscous device. For EQ1A, EQ1B and EQ2B the dampers deviate away from a linear response implying a dependency on stroke amplitude. This is very clear for EQ1B were the dampers exhibited a choppy yet consistence response. It is believed that this response is the result of possible air bubble formation around the moving damper pistons due to the high frequency strokes at model scale. Notwithstanding this, the dampers continue to exhibit a steady hysteretic behaviour and successfully add damping to the superstructure.

3.2 *Effects of input motion intensity*

To investigate different degrees of SSI, the intensity of the 0.8 Hz single-tone motion was increased. For the sake of comparison between two motions of different magnitudes, the

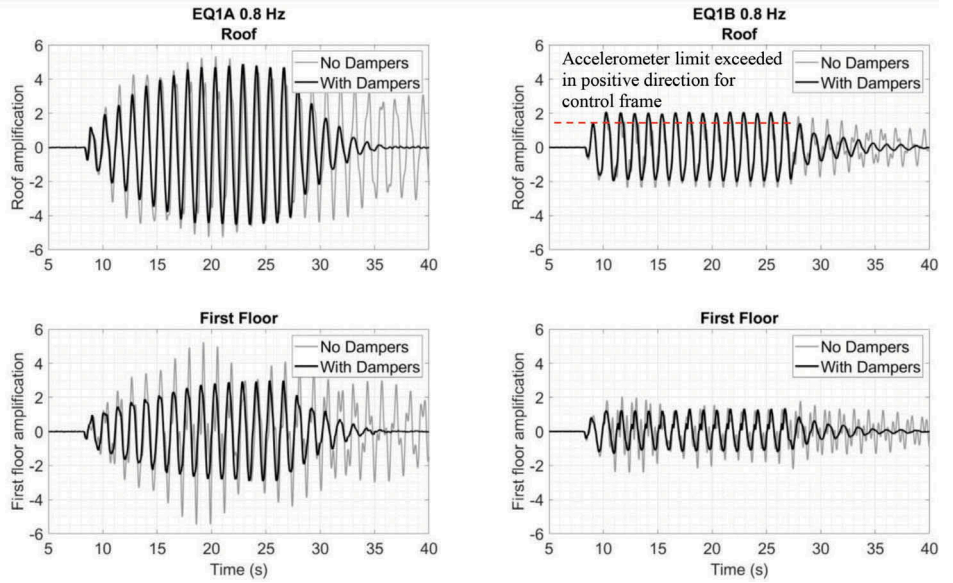

Figure 6. Amplification of floor accelerations relative to raft accelerations for EQ1A and EQ1B.

absolute floor accelerations in each frame were normalised relative to the raft accelerations during that specific motion. The resulting acceleration amplification traces for the 0.8 Hz input motions are presented in Figure 6. It is important to highlight that the MEMS accelerometer at the roof of the bare frame saturated in the positive direction during EQ1B (as shown by the dashed line in Figure 6). Hence, the positive amplification peaks at the roof of the control frame could not be fully captured. Nevertheless, the drop in floor amplification for both the damped frame and the control structure is very clear for higher earthquake intensities. In fact, the building without dampers had very similar floor amplification magnitudes as the damped structure during EQ1B. This implies similar levels of energy dissipation during the base motion. Given that the same linear elastic bare frame was used during both weak and strong motions, the reduction in floor acceleration amplification observed during EQ1B would only possible if an additional source of energy dissipation were to appear during the strong input motion. This source is believed to be the hysteretic sand beneath the foundation. The same reduction in floor amplification was observed for the case of the frame with dampers.

Figure 7 shows the ratio of peak damper stroke to the maximum interstory displacement for earthquakes of different intensity and frequency. Absolute floor displacements include raft motion (u_g), structural interstory drift (u_{str}), as well as the horizontal component due to rotation (u_θ); i.e. absolute floor displacement for floor "i" is defined as $u_i^{abs} = u_g + u_{str,i} + u_{\theta,i}$. For an ideal case where the frame is fixed at its base, the peak damper stroke at each floor should match the peak interstory drift (u_{str}) provided that the members connecting the damper to the frame are infinitely rigid. This is often the basis behind adopting a modal-based approach for predicting damper inputs in structures. For the real case of buildings on compliant ground, input into the dampers deviate away from this idealistic assumption as the horizontal component of building rotation (u_θ) influences damper strokes. Results in Figure 7 show that as the intensity of the input motions increases, a considerable drop in damper input is observed. This trend seems to be more noticeable for the damper higher up in the structure.

3.3 *Foundation-soil interaction*

The vertical accelerometers positioned at the base of both frames (RA1, RA2, RB1 and RB2 in Figure 2) provide valuable insight into foundation rotations. By dividing the difference

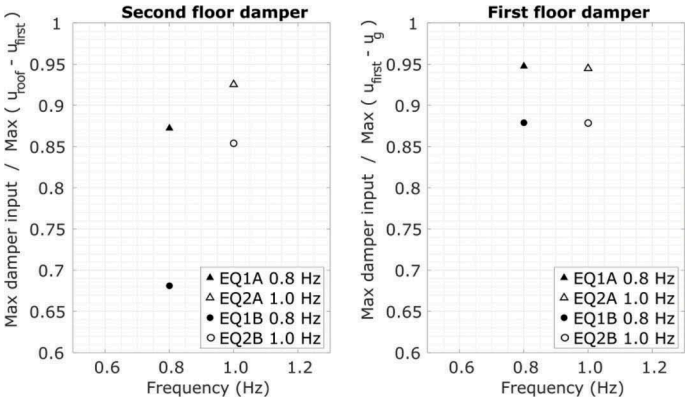

Figure 7. Ratio of peak damper stroke to peak interstory displacement for the input motions investigated.

between the two vertical accelerations on each side of the raft by the foundation width, data about the dynamic rotational accelerations of the rafts can be obtained. Through double integration and high-pass filtering, dynamic raft rotations can in turn be computed. Figure 8 presents normalised moment-rotation plots for the control and damped frames under the different input motions investigated. Inertial forces from the floors induce overturning moments on the raft which drive building rotations. The equations of motion presented in Kim et al. (2015) for a two degree of freedom structure have been used. The resulting moments are normalised by the critical moment needed to cause rotational instability for a rigid base condition (PL/2), were P is the frame weight and L/2 is half the frame width.

For the weak near-resonance input motion investigated (EQ1A), both the damped frame and the control frame exhibit rocking despite the squat aspect ratio of the buildings. In fact, it appears that the addition of dampers to the superstructure significantly reduces the energy dissipated at the raft-soil interface as depicted by the smaller hysteresis loop for the frame with dampers. The over-turning moments on the undamped frame raft seem to be converging to a limit governed by soil yielding and foundation uplift. These larger moments resulted in bigger rotations of the control frame which in turn induced noticeable degradation in soil stiffness beneath the raft. This is evident by the difference in gradient between the moment-rotation plots for the control frame and for the damped frame. As the intensity of the input motion is increased (EQ1B), a greater degree of nonlinearity is observed in the moment rotation plots

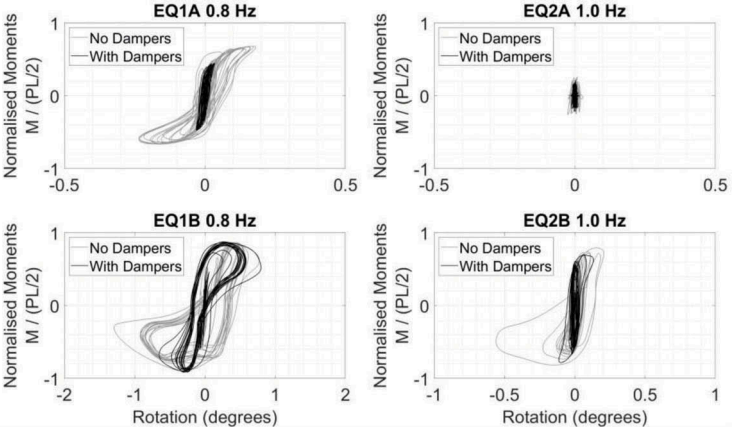

Figure 8. Dynamic raft rotations for the bare and the damped frames during the sinusoidal excitations.

for both structures. Most noticeably is the increase in the moment cap achieved during the earthquake. This increase is attributed to the densification of the sand beneath the foundations after successive base excitations.

It is believed that the global rocking response of both frames and the energy dissipation associated with it is what induced the drop in the floor amplification traces presented earlier in Figure 6. The two frames did not rock when triggered with EQ2A (weak input motion above resonant frequency of the buildings). However, as the intensity of input motion increased (EQ2B), the two buildings started rocking. This supports the conclusion that the observed drop in ratio of damper stroke to inter-story displacement in Figure 7 is indeed driven by structural rocking.

4 CONCLUSIONS

Successful implementation of model oil dampers in the centrifuge was presented. The devices were able to mitigate peak floor accelerations and drastically reduce free vibrations post-earthquake. The achieved damping ratio however needs to be increased slightly to mimic typical ratios obtained in prototype buildings with viscous dampers. The effects of earthquake intensity on the dynamic response of a bare frame and a damped frame have been investigated. The global rocking of the structures on sand adds damping to the overall soil-structure system. This ground compliance was found to reduce the damper performance relative to what the dampers would have experienced if the buildings were fixed to rigid ground. This finding raises the need for further testing on more slender building frames that would typically exhibit greater global rocking modes during earthquakes. The degree of SSI in this study was varied by controlling the intensity of the input motion. This can be also achieved by investigating soils with different degrees of stiffness.

REFERENCES

Boksmati, J.I., Madabhushi, S.P.G. & Thusyanthan, N.I. 2018. Development of model structural dampers for dynamic centrifuge testing. In A. McNamara, S. Divall, R. Goodey, N. Taylor, S. Stallebrass, J. Panchal (eds.), *Proc. 9th International Conference on Physical Modelling in Geotechnics (ICPMG 2018), Vol. 2, London, 17–20 July 2018*. Boca Raton, Florida: CRC Press.

Brennan, A.J., Madabhushi, S.P.G. & Houghton N.E. 2006. Comparing laminar and esb containers for dynamic centrifuge modelling. In C.W.W. Ng, Y.H. Wang & L.M. Zhang (eds.), *Proc. 6th International Conference on Physical Modelling in Geotechnics (ICPMG 2006), Hong Kong, 4-6 August 2006*. London: Taylor & Francis.

Chang, K.C., Lin Y.Y. & Chen C.Y. 2008. Shaking table study on displacement-based design for seismic retrofit of existing buildings using nonlinear viscous dampers. *Journal of Structural Engineering* 134(4): 671–681.

Chuanromanee, O., Hanson, R.D., Woods, R.D. 1995. The influence of soil-structure interaction on the overall damping of structures with high damping. *Transactions on the Built Environment, Soil Dynamics and Earthquake Engineering* 15: 575–582.

Haigh, S.K., Eadington, J. & Madabhushi, S.P.G. 2012. Permeability and stiffness of sands at very low effective stresses. *Geotechnique* 62(1): 69–78.

Ji, X., Hikino, T., Kasai, K. & Nakashima, M. 2013. Damping identification of a full-scale passively controlled five-story steel building structure. *Earthquake Engineering and Structural Dynamics* 42(2): 277–295.

Kim, D.K., Lee, S.H., Kim, D.S., Choo, Y.W. & Park, H.G. 2015. Rocking effect of mat foundation on the earthquake response of structures. *Journal of Geotechnical and Geoenvironmental Engineering* 141(1).

Lee, D. & Taylor D.P. 2001. Viscous damper development and future trends. *The Structural Design of Tall Buildings* 10: 311–320.

Li, P., Yang, J. & Lu, X. 2015. Study on Influence of vibration reduction effect of viscous dampers considering soil-structure dynamic interaction. In *Proc. 6th International Conference on Advances in Experimental Structural Engineering, University of Illinois, Urbana-Champaign, 1–2 August 2015*.

Madabhushi, S.P.G., Haigh, S.K. & Houghton, N.E. 2006. A new automated sand pourer for model preparation at University of Cambridge. In C.W.W. Ng, Y.H. Wang & L.M. Zhang (eds.), *Proc. 6th International Conference on Physical Modelling in Geotechnics (ICPMG 2006), Hong Kong, 4-6 August 2006*. London: Taylor & Francis.

Madabhushi, S.P.G., Haigh, S.K., Houghton, N.E. & Gould, E. 2012. Development of a servo-hydraulic earthquake actuator for the Cambridge Turner Beam Centrifuge. *International Journal of Physical Modelling in Geotechnics* 12(2): 77–88.

Madabhushi, S.P.G. 2014. *Centrifuge modelling for Civil Engineers*. Boca Raton, Florida: CRC Press.

Seleemah, A.A. & Constantinou, M.C. 1997. Investigation of seismic response of buildings with linear and nonlinear fluid viscous dampers. *Technical Report NCEER-97-0004, National Center For Earhquake Engineering Research, State University of New York at Buffalo*.

Zhou, Y., Guo, Y. & Zhu, Y. 2012. Influence of soil-structure interaction effects on the performance of viscous energy dissipation systems. In *Proc. 15th World Conference on Earthquake Engineering, Lisbon, 24–28 September 2012*.